Tyrosine Raman Signatures of the Filamentous Virus Ff Are Diagnostic of Non-Hydrogen-Bonded Phenoxyls: Demonstration by Raman and Infrared Spectroscopy of p -Cresol Vapor † , ‡

ARTICLE *in* BIOCHEMISTRY · FEBRUARY 2001

Impact Factor: 3.02 · DOI: 10.1021/bi0023753 · Source: PubMed

Tyrosine Raman Signatures of the Filamentous Virus Ff Are Diagnostic of Non-Hydrogen-Bonded Phenoxyls: Demonstration by Raman and Infrared Spectroscopy of *p*-Cresol Vapor[†,‡]

Zane Arp,[§] Daniel Autrey,[§] Jaan Laane,[§] Stacy A. Overman,[||] and George J. Thomas, Jr.*[,||]

Department of Chemistry, Texas A&M University, College Station, Texas 77843-3255, and School of Biological Sciences, University of Missouri—Kansas City, Kansas City, Missouri 64110-2499

Received October 12, 2000; Revised Manuscript Received December 21, 2000

ABSTRACT: *p*-Cresol is a simple molecular model for the *para* phenolic side chain of tyrosine. Previously, Siamwiza and co-workers [(1975) *Biochemistry 14*, 4870−4876] investigated *p*-cresol solutions to identify Raman spectroscopic signatures for different hydrogen-bonding states of the tyrosine phenoxyl group in proteins. They found that the phenolic moiety exhibits an intense Raman doublet in the spectral interval 820−860 cm^{-1} and that the doublet intensity ratio (I_2/I_1, where I_2 and I_1 are Raman peak intensities of the higher- and lower-wavenumber members of the doublet) is diagnostic of specific donor and acceptor roles of the phenoxyl OH group. The range of the doublet intensity ratio in proteins ($0.30 < I_2/I_1 < 2.5$) was shown to be governed by Fermi coupling between the phenolic ring-stretching fundamental ν_1 and the first overtone of the phenolic ring-deformation mode ν_{16a}, such that when the tyrosine phenoxyl proton is a strong hydrogen-bond donor, $I_2/I_1 = 0.30$, and when the tyrosine phenoxyl oxygen is a strong hydrogen-bond acceptor, $I_2/I_1 = 2.5$. Here, we interpret the Raman and infrared spectra of *p*-cresol vapor and extend the previous correlation to the *non-hydrogen-bonded* state of the tyrosine phenoxyl group. In the absence of hydrogen bonding, the Raman intensity of the higher-wavenumber component of the canonical Fermi doublet is greatly enhanced such that $I_2/I_1 = 6.7$. Thus, for the non-hydrogen-bonded phenoxyl, the lower-wavenumber member of the Fermi doublet loses most of its Raman intensity. This finding provides a basis for understanding the anomalous Raman singlet signature (∼854 cm^{-1}) observed for tyrosine in coat protein subunits of filamentous viruses Ff and Pf1 [Overman, S. A., et al. (1994) *Biochemistry 33*, 1037−1042; Wen, Z. Q., et al. (1999) *Biochemistry 38*, 3148−3156]. The implications of the present results for Raman analysis of tyrosine hydrogen-bonding states in other proteins are considered.

The efficacy of Raman spectroscopy as a structural probe of proteins requires definitive vibrational assignments for spectral bands associated with specific secondary structures of the peptide main chain and specific local environments of the side chains. Among the earliest Raman markers established as diagnostic of protein side chain environment are those occurring in the 820−860 cm^{-1} interval (*1*). In a classic 1975 paper, Siamwiza and co-workers (*2*) demonstrated that the pair of tyrosine Raman markers centered at approximately 830 and 850 cm^{-1} in globular proteins represents a Fermi-interaction doublet arising from energy level coupling between the normal mode ν_1[1] (ring-breathing fundamental) and the second harmonic $2\nu_{16a}$ (ring-deformation overtone) of the *para*-substituted phenolic side chain. If Fermi interaction is very weak or absent, only the uncoupled ν_1 mode would be expected to exhibit a Raman band of appreciable intensity in the 820−860 cm^{-1} interval (i.e., $I_2/I_1 \sim 10$). Siamwiza and co-workers (*2*) further demonstrated that the relative Raman intensity ratio I_2/I_1 (where I_2 and I_1 are the peak intensities of the higher- and lower-wavenumber members of the doublet, respectively) is strongly dependent upon the hydrogen-bonding state of the tyrosine phenoxyl group. Thus, in proteins, when the phenoxyl proton is the donor of a strong hydrogen bond, it is found that I_2/I_1 is approximately equal to 0.30; conversely, when the phenoxyl oxygen is the acceptor of a strong hydrogen bond, then I_2/I_1 approaches 2.5. If the phenoxyl group acts as both a donor and an acceptor of hydrogen bonds, as is expected for a solvent-exposed tyrosine, then I_2/I_1 is approximately 1.25.

The similarity of *p*-cresol (I) to the phenolic moiety of tyrosine (II) makes it an ideal model compound for understanding the vibrational modes of the tyrosyl side chain.

[†] Supported by Grant GM50776 from the National Institutes of Health (to G.J.T.) and by grants from the National Science Foundation and Robert A. Welch Foundation (to J.L., Z.A., and D.A.).

[‡] Part LXXI in the series Structural Studies of Viruses by Raman Spectroscopy.

* To whom correspondence should be addressed.

[§] Texas A&M University.

[||] University of Missouri-Kansas City.

[1] Abbreviations: UVRR, ultraviolet resonance Raman; ν_1, in-plane breathing fundamental of the *para*-substituted phenyl ring; ν_{16a}, out-of-plane deformation fundamental of the *para*-substituted phenyl ring; $\{\nu_1; 2\nu_{16a}\}$, Fermi-coupled vibrational modes due to resonance interaction between ν_1 and the first overtone of ν_{16a}; I_2/I_1, Raman peak intensity ratio of the Fermi doublet $\{\nu_1; 2\nu_{16a}\}$, where I_2 and I_1 represent higher- and lower-wavenumber members of the doublet, respectively; A_1, A_2, B_1, and B_2, symmetry species of point group C_{2v}; Ff, class I filamentous virus (includes strains fd, f1, and M13); Pf1, Pf3, and Xf, class II filamentous viruses.

10.1021/bi0023753 CCC: $20.00
Published on Web 01/30/2001

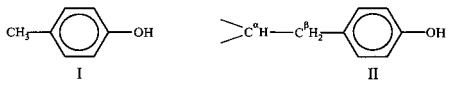

I II

Takeuchi, Watanabe, and Harada (*3*) investigated the Raman and infrared spectra of *p*-cresol and several of its deuterated species in solution and carried out normal coordinate calculations. Their results support the correlation of Siamwiza and co-workers (*2*), which is now widely accepted for characterizing tyrosine environments in soluble globular proteins (*4*−*6*). A similar correlation may also hold for the near-UV resonance Raman (UVRR) spectra (*7*). In the case of nonglobular proteins, however, the structural significance of the I_2/I_1 parameter has not been rigorously assessed. For example, the literature contains no report of the measurement of I_2/I_1 for a tyrosyl side chain meeting both of the following criteria: (1) the side chain is buried within a transmembrane α-helix, and (2) the local hydrogen-bonding environment of the phenolic OH group is known from an independent structural determination.

Overman and co-workers (*8*−*10*), using both site-directed mutagenesis and tyrosine-specific isotope labeling of the filamentous bacteriophage Ff, presented definitive evidence that neither of the two tyrosyl side chains (Tyr 21 and Tyr 24) of the 50-residue α-helical coat protein subunit generates the canonical Fermi doublet observed for tyrosines in other proteins. Instead, Tyr 21 exhibits a single prominent Raman band at 851 ± 1 cm^{-1}, and Tyr 24 exhibits a single prominent band at 855 ± 1 cm^{-1}. Apparent singlets, rather than doublets, are also observed in the 229 nm excited UVRR spectrum of Ff (*11*). Such singlets are unprecedented and indicate a heretofore uncharacterized local environment for tyrosine phenoxyls in the native viral capsid. Interestingly, Tyr 21 and Tyr 24 are located in a highly hydrophobic segment of the subunit α-helix. Prior to virion assembly, this region of the subunit can be protected from polar interactions by sequestration within the host cell membrane (*12*, *13*). Once the subunits are incorporated into the extensively overlapped and interdigitated superhelical array of the mature Ff virion (*14*, *15*), the tyrosines presumably remain shielded from polar interactions. Biophysical studies confirm that coat subunits of Ff do not retain their native α-helical secondary structure unless incorporated within the assembled virion or solubilized in membrane-like phospholipid bilayers or detergent micelles (*16*, *17*).

Overman and Thomas (*9*, *10*) concluded that the anomalous Raman singlets exhibited by both Tyr 21 and Tyr 24 in subunits of the native Ff assembly might be indicative of a highly hydrophobic local environment for each phenoxyl group, a state not represented in any previously studied model compound or globular protein. This is compatible with membrane sequestration prior to assembly, as well as with tight packing of subunits in the mature virion. To further test this hypothesis, we have investigated the Raman spectrum of the tyrosyl model compound, *p*-cresol, in a simulated hydrophobic environment, viz., in the vapor phase at elevated temperature (∼300 °C). Intermolecular associations, including phenoxyl hydrogen bonding, should be minimal or completely absent under these conditions. In addition, we have investigated the infrared spectrum of *p*-cresol in the vapor state (∼200 °C) to attain a comprehensive understanding of the vibrations of this molecule when intermolecular interactions are absent. Raman and infrared spectra of *p*-cresol liquid have also been re-examined for comparison with the newly obtained vapor phase data. Finally, *ab initio* calculations have been carried out on *p*-cresol to support vibrational assignments of the Raman and infrared spectral bands. The results reveal a novel vibrational signature for tyrosine that is relevant not only to filamentous virus architecture but also to other applications of Raman spectroscopy in the structural analysis of tyrosine-containing proteins.

EXPERIMENTAL PROCEDURES

p-Cresol (99%) was purchased from Aldrich Chemical (St. Louis, MO). Raman spectra were collected on a Jobin Yvon U-1000 spectrometer (Instruments S. A., Edison, NJ) using excitation at 514.5 nm from an Innova 20 argon-ion laser (Coherent, Santa Clara, CA). The laser power at the sample cell was 2 W for vapor and 800 mW for liquid samples. Vapor phase spectra were obtained at 300 ± 5 °C using a custom-designed, thermostatically controlled Raman cell (*18*) into which *p*-cresol liquid was injected; the Raman cell was subsequently frozen with liquid nitrogen and sealed after evacuation on a vacuum line. Liquid phase spectra were obtained at 22 ± 0.5 °C. Either a charge-coupled device or a photomultiplier tube was used for detection of the Raman scattered light. The Raman spectra were collected and processed using standard software packages.

Infrared spectra were recorded on either a Bomem DA8.02 or a BioRad FTS-60 instrument. Vapor phase spectra at 200 ± 10 °C were recorded using a heatable 10 cm metal cell with KBr windows. Liquid samples (melts) between KBr plates were recorded at 45 °C.

RESULTS

Experimental and Theoretical Vibrational Spectra of p-Cresol. A comprehensive tabulation of Raman and infrared band frequencies, relative intensities, and assignments for the *p*-cresol molecule in liquid and vapor states is given in Table 1. Included for comparison are previously reported experimental data, as well as the results of normal coordinate analysis and *ab initio* calculations. The assignments (left column) are based upon approximate C_{2v} symmetry, which should be followed quite closely for normal modes of the *para*-substituted phenyl ring, assuming relatively free rotations of the exocyclic CH_3 and OH substituents. Localized vibrations of the CH_3 and OH groups are listed separately in Table 1 (bottom section), with the exception of the totally symmetric vibrations of symmetry species A_1 (top section). Because the C_{2v} symmetry is only approximate, several of the CH_3 and OH vibrations cannot be readily classified according to this point group and have not been numbered in the conventional manner. However, we indicate the two vibrations corresponding to modes designated previously (*2*) as ν_1 and ν_{16a}.

Raman Spectrum of p-Cresol Liquid. Figure 1 shows the Raman spectrum of *p*-cresol liquid (22 °C). The spectral bands of the 300−1800 cm^{-1} interval are virtually identical to those previously reported and analyzed in detail (*2*, *3*). Of particular interest is the weak Raman band at 416 cm^{-1}, assigned previously and presently to an out-of-plane ring-

Table 1: Experimental and Calculated Vibrational Frequencies of *p*-Cresol

			IR vapor[b]		IR liquid[b]		Raman liquid[c]		lit.		this work	
	approximate description[a]	Raman vapor[c]	this work	lit.[d]	this work	lit.[d]	this work	lit.[d]	CASSCF[e]	B3LYP 6-31+G[f]	B3LYP 6-311++G**	scaling factor
A_1	O−H stretch	3654 (30)	3654	3713	3333[g] vs	3344[g]	3370[g] (1) 3337[g] (1) 3504[g] (1)	−	3711	3611	3838	0.952
	C−H stretch	3061[h] (48)	−	3067[h]	3062[h] w	3058[h]	3061[h] (24)	3057[h]	3095	3033	3191	0.959
	C−H stretch	3061[h] (48)	−	3067[h]	3062[h] w	3058[h]	3061[h] (24)	3057[h]	3049	2998	3167	0.967
	CH_3 sym stretch	2881 (22)	2880 w	−	2866 mw	−	2867 (19)	−	2900	2865	3021	0.953
	C−C stretch	1618 (6)	1612 ms	1621	1615 ms	1618	1616 (42)	1612	1624	1622	1656	0.973
	C−C stretch	1517 (1)	1516 s	1520	1514 vs	1515	1515 (3)	−	1537	1519	1545	0.981
	CH_3 sym deformation	1385 (8)	−	−	1380 vw	1379	1382 (34)	1380	1436	1384	1415	0.979
	C−O stretch	1256 (20)	1258 s	1255	1238 vs	1235	1255 (11)	1251	1245	1258	1274	0.987
	CH_3 stretch	1215 (16)	−	−	1213 vw	−	1217 (29)	1212	1194	1180	1229	0.989
	C−H wag	1172 (17)	1172 s	1178	1171 m	1172	1174 (28)	1170	1128	1161	1195	0.981
	C−H wag	1008 (2)	1010 vw	1015	1016 w	1016	1018 (3)	1011	1008	982	1031	0.987
	C−C stretch (ν_1)	839 (100)	840 vvw	−	841 ms	841	844 (100)	842	823	833	851	0.986
	ring-bending	737 (6)	738 m	739	738 ms	−	742 (6)	740	727	736	745	0.991
	ring-bending	460 (51)	459 w	459	462 w	464	466 (56)	468	459	459	467	0.983
	$2\nu_{16a}$	812 (15)	−	−	−	823	824 (35)	823	−	−	−	−
A_2	C−H wag (op)	953 (1)	−	−	954	952	957 (1)	−	952	962	962	0.991
	C−H wag (op)	−	−	−	−	−	−	−	824	830	830	0.987
	ring-bending (op) (ν_{16a})	−	−	−	−	−	416[h] (3)	416[h]	416	414	419	0.995
B_1	C−H wag (op)	918 (1)	−	−	927 w	926	927 (1)	928	936	921	919	0.999
	C−H wag (op)	−	819 s	811	815 vs	816	−	−	805	804	804	1.019
	ring-bending (op)	−	699 w	698	703 w	702	703 (11)	700	698	693	693	1.009
	ring-bending (op)	−	504 s	503	508 s	508	510 (4)	512	510	504	513	0.982
	C−O wag (op)	−	−	294	−	−	−	−	333	321	331	0.888
	C−CH_3 wag (op)	−	−	−	−	−	−	161	157	146	144	−
B_2	C−H stretch	3039 sh	3029[h] ms	−	3033 ms	3036	3039 (44)	3037[h]	3064	3007	3157	0.959
	C−H stretch	3016 (23)	3029[h] ms	−	3024 ms	3024	3013 (33)	3037[h]	3042	2986	3146	0.963
	C−C stretch	−	−	−	1600 s	1600	1602 (35)	1612	1599	1596	1632	0.980
	C−C stretch	−	1428 m	1431	1437 ms	1437	−	−	1456	1430	1456	0.981
	C−C stretch	1334 (1)	1334 m	1337	1363 m	1369	1330 (1)	−	1366	1329	1359	0.982
	C−H wag	1298 (1)	−	−	1298 w	1298	1298 (7)	1290	1294	1297	1332	0.974
	C−H wag	1114 (1)	−	1114	1116 vw	?	1114 (3)	1112	1077	1102	1129	0.987
	ring-bending	644 (4)	644 vw	642	645 vw	−	646 (79)	642	657	643	657	0.980
	C−O wag	−	416 vw	420	416 vw	416	416[h] (3)	416[h]	430	422	426	0.977
	C−CH_3 wag	328 (5)	−	333	339 mw	339	339 (57)	341	313	304	304	1.079
other CH_3 and OH modes	CH_3 antisym stretch	2934 (51)	2935 m	2915	2922 ms	2922	2915 (45)	2919	2973	2942	3098	0.947
	CH_3 antisym stretch	2934 (51)	2935 m	2915	2922 ms	2922	2915 (45)	2919	2953	2914	3067	0.957
	CH_3 antisym deformation	1472 (1)	−	−	1463 w	1463	1464 (7)	1458	1519	1465	1502	0.980
	CH_3 antisym deformation	1472 (1)	−	−	1463 w	1463	1464 (7)	1458	1513	1447	1487	0.990
	CH_3 rock	−	1104 m	1105	1105 ms	1107	1109 (3)	−	1073	1035	1060	1.042
	CH_3 rock	−	−	−	1042 w	1042	1042 (2)	1032	1027	1009	1001	1.041
	CH_3 torsion	−	−	−	−	−	−	−	65	−	18	−
	O−H wag (ip)	1187 (12)	−	−	−	−	−	−	1214	1217	1185	1.002
	O−H wag (op)	−	−	294 s	−	−	−	−	294	297	296	0.993

[a] Only the principal contribution is shown; several vibrations are strongly coupled. Abbreviations: op, out-of-plane; ip, in-plane. [b] Abbreviations: s, strong; m, medium; w, weak; v, very. [c] Relative intensities in parentheses are on arbitrary 1−100 scale. Abbreviation: sh, shoulder. [d] Literature values from ref *21*. [e] From reference *23*. [f] From reference *24*. [g] Hydrogen-bonded species. [h] Wavenumber values used twice.

bending mode of symmetry type A_2 (ν_{16a} in ref *2*). The present *ab initio* calculation (Table 1 and *Ab Initio* Calculation below) predicts that two normal modes of vibration occur in the neighborhood of 420 cm^{-1}. The first is the A_2 ring-bending mode (ν_{16a}), for which the predicted wavenumber is 419 cm^{-1} and the predicted band intensity is moderate in the Raman but negligible in the infrared; the second is a C−OH wagging mode with B_2 symmetry, for which the predicted wavenumber is 426 cm^{-1} and the predicted Raman intensity is negligible. Interestingly, the *ab initio* calculation predicts that the B_2 C−OH wagging mode should have observable infrared intensity, as will be discussed below (Infrared Spectra of *p*-Cresol Liquid and Vapor).

Takeuchi and co-workers (*3*) reported Raman spectra of the *o*-dideuterio- and tetradeuteriophenoxyl isotopomers of *p*-cresol in solution and demonstrated that ν_{16a} shifts to 368 and 372 cm^{-1}, respectively, as expected for the A_2 ring-bending mode. Conversely, the B_2 C−OH mode was shown to exhibit much smaller deuterium isotope shifts. The relevance of these assignments is that the overtone of the A_2 ring-bending mode ($2\nu_{16a}$) undergoes energy-level interaction (Fermi resonance) with the symmetric skeletal stretching

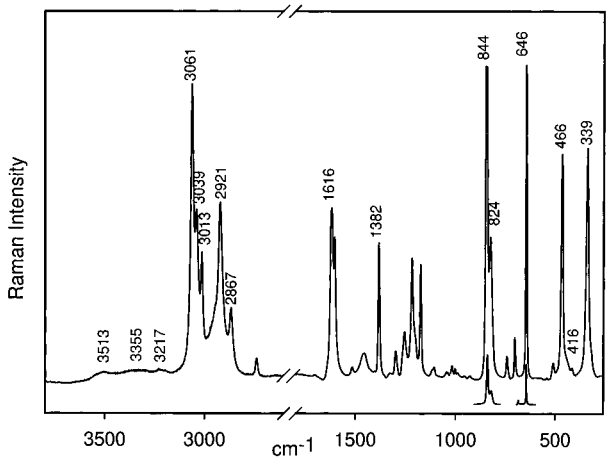

FIGURE 1: Raman spectrum of *p*-cresol liquid at 22 °C obtained with 514.5 nm excitation (800 mW) in the regions 300−1800 (charge-coupled-device detection) and 2800−3800 cm^{-1} (photomultiplier detection). Insets (1:10 intensity reduction) show the full intensity profiles of the truncated bands at 646 and 844 cm^{-1}.

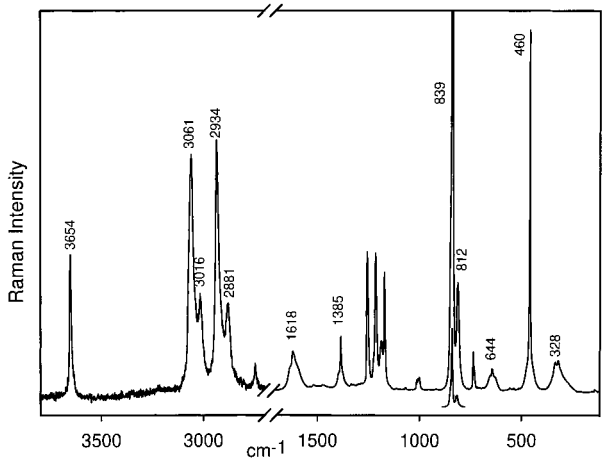

FIGURE 2: Raman spectrum of *p*-cresol vapor (600 Torr) at 300 °C obtained with 514.5 nm excitation (2 W) in the regions 300−1800 (charge-coupled-device detection) and 2800−3800 cm^{-1} (photomultiplier detection).

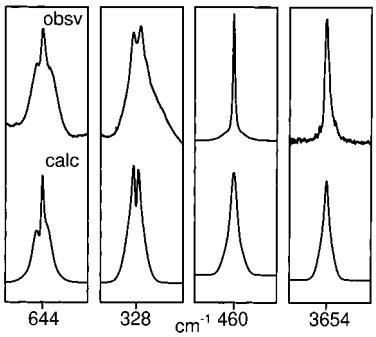

FIGURE 3: Observed (top) and calculated (bottom) contours of representative Raman bands in the vapor phase spectrum of *p*-cresol at 300 °C. Shown from left to right are the bands centered near 644, 328, 460, and 3654 cm^{-1}. These are typical of the different Raman band contours expected for the *p*-cresol molecule (*20*).

mode of the phenyl moiety (ring-breathing mode with A_1 symmetry) to produce the Fermi doublet with components near 824 and 844 cm^{-1} in *p*-cresol liquid. The results of Takeuchi and co-workers (*3*) show that the B_2 C−OH wagging mode is not involved in the Fermi interaction. Also in accord with the previous work (*2*, *3*), our measurements indicate that $I_2/I_1 = 3.6$ for *p*-cresol liquid. This is considered diagnostic of strong hydrogen-bond acceptance by the phenolic oxygen atom of *p*-cresol in the liquid state and is close to the "canonical" maximum value ($I_2/I_1 = 2.5$) for a similarly hydrogen-bonded tyrosine in a globular protein (*2*).

In the 2600−3800 cm^{-1} interval, the spectrum of Figure 1 is dominated by bands due to C−H stretching vibrations of the exocyclic methyl group (2867 and 2921 cm^{-1}) and aromatic hydrogens (3013, 3039, and 3061 cm^{-1}). What appear to be weak overtones may also contribute near 3200 cm^{-1}. Of particular interest, and not reported previously, is the phenoxyl O−H bond stretching vibration. The O−H stretching band is expected within the 3300−3700 cm^{-1} interval, with the precise position determined by the hydrogen-bonding state of the phenoxyl proton. In Figure 1, the O−H bond stretching vibration is represented by three very broad and weak bands centered near 3217, 3355, and 3513 cm^{-1}. The observed frequencies, intensities, and contours are indicative of significant hydrogen-bonding interactions of the phenoxyl proton (*19*). Because we find no spectral or chromatographic evidence of contamination of *p*-cresol liquid with water or other hydrogen-bonding agents, we conclude that the appearance of three distinct bands is due to participation of the phenoxyl proton in several spectroscopically distinguishable types of intermolecular hydrogen bonds. For example, strong hydrogen bonding to a phenoxyl oxygen acceptor and weaker hydrogen bonding to the π-electron system of the phenolic ring could produce different O−H stretching bands. Dimers, trimers, and higher oligomers may also generate distinguishable Raman markers.

Raman Spectrum of p-Cresol Vapor. Figure 2 shows the Raman spectrum of *p*-cresol vapor (300 °C). Raman band contours of several different types are expected in vapor phase spectra, depending upon the symmetry type of the normal mode and related structural factors. Although the Raman band contours can be calculated, the calculated results may differ from the observed contours for various reasons (S. Sakurai and J. Laane, unpublished results) (*20*). In the case of *p*-cresol vapor, some hybridization of the calculated contours is expected, because the molecular symmetry is lower than C_{2v}. In addition, contours of low-energy vibrational bands can be perturbed by significant population of excited vibrational energy levels at 300 °C, which leads to the simultaneous appearance of both the fundamental band and partially overlapping "hot" bands. For these reasons, only qualitative or semiquantitative agreement can be expected between calculated and experimental Raman band contours of *p*-cresol at 300 °C. This is illustrated in Figure 3, which compares four of the observed vapor phase Raman bands with their corresponding calculated contours. Given the foregoing considerations, the agreement is highly satisfactory and adds validity to the assignments and following interpretations.

Most of the Raman bands observed in the vapor phase spectrum of *p*-cresol (Figure 2) have identifiable counterparts in the liquid phase spectrum (Figure 1) and are assigned accordingly (*2*, *3*), as shown in Table 1. However, the following major differences between vapor and liquid are noteworthy. First, the vapor phase spectrum exhibits no Raman intensity in the 3300−3600 cm^{-1} interval that could be considered diagnostic of hydrogen bonding by the

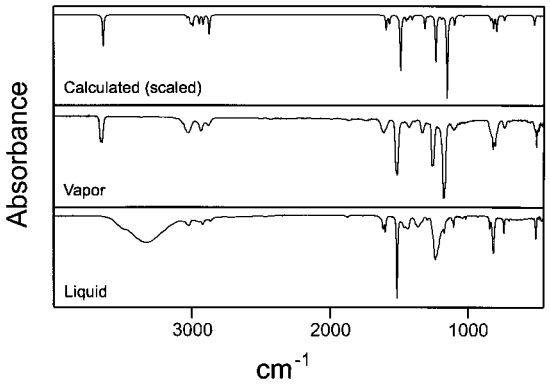

FIGURE 4: Comparison of the observed infrared absorption spectra of *p*-cresol liquid (bottom) and vapor (middle) with the scaled *ab initio* calculation of infrared intensities in the gas phase (top). The *ab initio* calculation was conducted at the B3LYP 6-311++G** level (*22*).

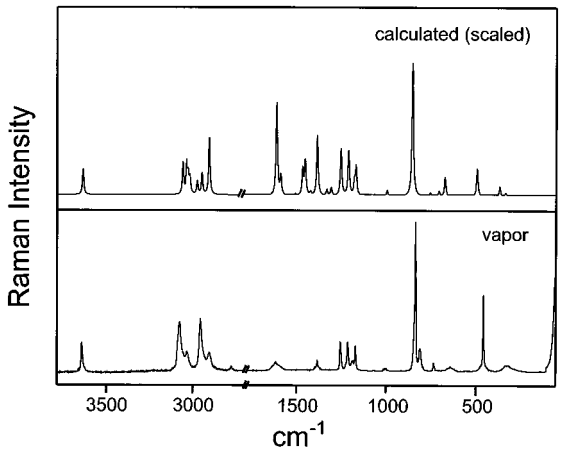

FIGURE 5: Comparison of the observed Raman spectrum of *p*-cresol vapor (bottom) with the scaled *ab initio* calculation of Raman intensities in the gas phase (top). The *ab initio* calculation was conducted at the B3LYP 6-311++G** level (*22*). Note that the Fermi doublet at 839/812 cm^{-1} in the vapor spectrum is absent from the calculated spectrum. The latter exhibits instead a single band at 851 cm^{-1} that can be assigned to the A_1 ring-breathing mode (see explanation in text).

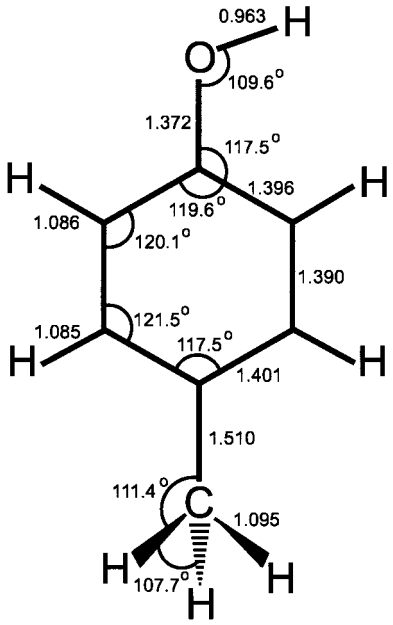

FIGURE 6: Structure of *p*-cresol calculated at the B3LYP 6-311++G** level (*22*). Bond lengths are in angstroms.

phenoxyl proton. Instead, a strikingly strong and sharp Raman band occurs at 3654 cm^{-1}. This band can be assigned unequivocally to the phenoxyl OH group of *p*-cresol (*19*) and demonstrates that the phenolic O−H proton is not engaged in an intermolecular hydrogen bond in the vapor phase at 300 °C. Second, *p*-cresol vapor does not exhibit the canonical Fermi doublet intensity ratio that is expected in the 820−860 cm^{-1} interval and observed for the liquid (Figure 1). Instead, a very strong band is observed at 839 cm^{-1}, and a very weak companion is observed at 812 cm^{-1} (Figure 2). Although the bands at 839 and 812 cm^{-1} do reflect a Fermi doublet, their peak intensity ratio (I_2/I_1 = 6.7) greatly exceeds the previously proposed limit (*2*).

Other Raman bands of the vapor phase spectrum that differ appreciably from their counterparts in the liquid phase spectrum are those at 328, 644, 1385, and 1618 cm^{-1}. In each case, the band is weak and displays a broadened contour due to rotational structure in the vapor phase, but intense and strongly polarized in the liquid phase. All have been assigned to in-plane vibrations of the *para*-substituted phenyl group (*3*).

Infrared Spectra of p-Cresol Liquid and Vapor. Infrared spectra of *p*-cresol in the liquid (22 °C) and vapor (200 °C) states are compared in Figure 4 with the *ab initio*-calculated spectrum. As is evident in Table 1, the infrared spectrum of the liquid is in substantial agreement with previously published results (*21*). It is important to note that vibrations of symmetry species A_2, which are infrared forbidden in strict C_{2v} symmetry, are not expected to exhibit appreciable intensity in the spectra of Figure 4. This includes the A_2 ring-bending mode (ν_{16a}), the first overtone of which has the potential for Fermi resonance with the A_1 ring-breathing fundamental (ν_1). Although infrared spectra of both the liquid and vapor states exhibit a weak band near 416 cm^{-1}, this band arises not from the infrared-forbidden A_2 fundamental but from the B_2 wagging mode of the exocyclic C−OH group. This assignment is supported by the *ab initio* calculation (next section), which predicts moderate infrared intensity and negligible Raman intensity for the B_2 C−OH wagging mode and vice versa for the A_2 ring-bending mode.

Ab Initio Calculation. To support the empirical vibrational assignments listed in Table 1, we employed Gaussian 98 (*22*) at the B3LYP 6-311++G** level for the *ab initio* calculation of vibrational (infrared and Raman) spectra of the *p*-cresol molecule. The calculated vibrational frequencies and scaling factors required to fit the experimental data are included in Table 1, and the calculated spectra are included in Figures 4 (infrared) and 5 (Raman). The scaling factors range from 0.950 for the highest-wavenumber band (O−H stretching vibration) to ∼0.99 for other bands. The calculated structure is shown in Figure 6. The *ab initio* results are in excellent overall agreement with both the experimental data presented here, previous normal coordinate calculations (*3*), and previous *ab initio* calculations (*23*, *24*), and provide additional information about the internal coordinates associated with each vibrational mode.

We have also computed the theoretical Raman spectrum (intensity vs wavenumber) for *p*-cresol, using the scaling factors listed in Table 1. The computed and experimental Raman spectra are compared in Figure 5. Although the

computation is for a vapor phase non-hydrogen-bonded molecule, the band contours were calculated utilizing Lorentzian band shapes rather than by simulation of vapor phase contours. Hence, full agreement between calculated and observed band shapes or peak intensities is not expected. On the whole, however, the agreement in frequencies and intensities is satisfactory. It should also be noted that the *ab initio* calculation yields only the fundamental vibrational modes of the vapor phase molecule; neither overtones nor overtone−fundamental coupling interactions are computed. Accordingly, while the experimental vapor phase spectrum exhibits the 812 cm^{-1} band (lower-wavenumber member of the Fermi doublet), the computed spectrum does not. This provides additional support for assignment of the 812 and 839 cm^{-1} couplet in the experimental vapor phase spectrum to a Fermi interaction doublet.

DISCUSSION

Structural Significance of the Tyrosyl Raman Signature in the 820−860 cm^{-1} Interval. The *p*-cresol molecule in the vapor phase is proposed as a model for the non-hydrogen-bonded state of the phenolic group, with application to the tyrosyl side chain in proteins. The validation of the model is demonstrated by the Raman band of very high wavenumber (3654 cm^{-1}) and very narrow width (*19*) observed for the phenolic O−H stretching vibration of *p*-cresol vapor, as seen in Figure 2.

In the spectral interval 820−850 cm^{-1}, the vapor phase Raman spectrum of *p*-cresol is distinguished by a Fermi doublet consisting of a very strong (839 cm^{-1}) and a very weak (812 cm^{-1}) component in lieu of the typical Fermi doublet diagnostic of phenoxyl hydrogen-bonding interactions in *p*-cresol liquid and in tyrosine-containing globular proteins (*2*, *4*, *5*). The Fermi doublet of *p*-cresol vapor thus exhibits an extraordinarily large peak intensity ratio ($I_2/I_1 = 6.7$) in comparison to *p*-cresol liquid ($I_2/I_1 = 3.6$) and hydrogen-bonded tyrosines in globular proteins ($0.30 < I_2/I_1 < 2.5$). The results presented here indicate that a non-hydrogen-bonded tyrosine phenoxyl should exhibit a Fermi doublet with $I_2/I_1 \gg 2.5$, likely approaching a value of 6 or 7. In addition, because I_2 is so much greater than I_1, the diagnostic Raman signature of such a non-hydrogen-bonded tyrosine may appear as a singlet rather than as a doublet. This is particularly likely for a protein or viral protein assembly yielding a Raman spectrum of limited signal-to-noise ratio.

We propose that in the absence of phenoxyl hydrogen bonding, Fermi coupling between ν_1 and the first overtone of the out-of-plane ring-deformation mode ($2\nu_{16a}$) is considerably weaker than in the presence of hydrogen bonding.

Extension of the Previously Proposed Correlation of Siamwiza et al. (2). The Fermi doublet diagnostic of the non-hydrogen-bonded phenolic moiety exhibits a Raman peak intensity ratio ($I_2/I_1 = 6.7$) that is clearly distinguishable from the range identified by Siamwiza et al. (*2*) as diagnostic of hydrogen-bonded tyrosines ($0.3 < I_2/I_1 < 2.5$). Accordingly, the results presented here provide a definitive empirical basis for characterizing the novel non-hydrogen-bonded phenoxyl environment from the conventional hydrogen-bonding environments prevalent in globular proteins. Importantly, the current findings suggest a basis for structural interpretation

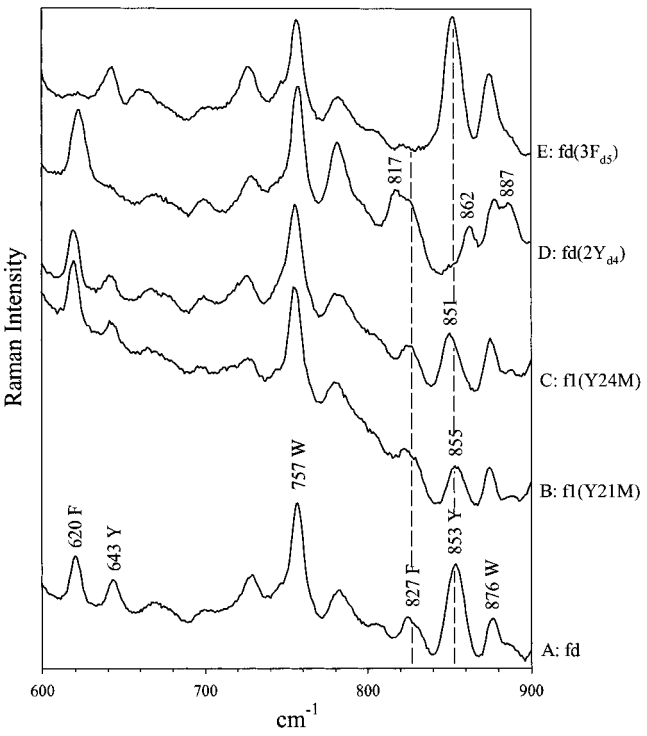

FIGURE 7: Raman spectra in the region 600−900 cm^{-1} of isotopic and mutant variants of the Ff filamentous virus demonstrating assignment of the prominent bands near 853 cm^{-1} to tyrosine and those near 827 cm^{-1} to phenylalanine. From bottom to top, wild-type unlabeled fd virus (A), mutant f1 virus in which Met replaces Tyr 21 (B), mutant f1 virus in which Met replaces Tyr 24 (C), wild-type fd in which phenolic rings of Tyr 21 and Tyr 24 are deuterated (D), and wild-type fd in which phenyl rings of Phe 11, Phe 42, and Phe 45 are deuterated (E). Note that the Raman bands of the two mutants, at 855 (B) and 851 cm^{-1} (C), respectively, are about half as intense as their composite in the wild-type virus at 853 cm^{-1} (A). Because the 827 cm^{-1} band is virtually completely removed by phenylalanine deuteration (E), it is assigned to Phe not Tyr. The 853 → 817 cm^{-1} deuteration shift and the absence of an 827 cm^{-1} deuteration shift (D) establish the singlet-like tyrosine markers for Tyr 21 and Tyr 24. Further details are given in refs *8* and *9*.

of the anomalous Raman signatures observed for coat protein tyrosines of the filamentous viruses Ff (*8*) and Pf1 (*25*), as discussed in the next section.

Tyrosyl Raman Markers in Coat Proteins of Filamentous Viruses. In the case of Ff (strains fd, f1, and M13), each of the two tyrosines of the coat subunit is known to generate a single strong Raman band in the 820−860 cm^{-1} interval of the Raman spectrum (*8*, *9*), in lieu of a canonical Fermi doublet (*2*). The apparent Raman "singlets" occur at 851 cm^{-1} for Tyr 21 and 855 cm^{-1} for Tyr 24 (*9*). This finding is supported by both site-directed mutagenesis of Tyr 21 and Tyr 24 (individually and in combination) and residue-specific deuterations of coat protein tyrosines and phenylalanines, as shown in Figure 7. Importantly, the data depicted in Figure 7 demonstrate that the three phenylalanines of the Ff coat subunit account for virtually all of the Raman intensity of Ff at 827 cm^{-1}. On the basis of these results, the previously reported (*8*) tyrosyl signatures of Ff, wherein $I_2 \gg I_1$, can be interpreted structurally as diagnostic of non-hydrogen-bonded phenoxyl groups in the native virion assembly.

The coat subunit of the Ff assembly is the first native protein for which a non-hydrogen-bonded tyrosine phenoxyl has been identified. The absence of phenoxyl group hydrogen

bonding in Ff may be attributed to the location of the tyrosines within a highly hydrophobic segment of the subunit sequence that represents part of the tightly packed subunit interface of the viral capsid. Indeed, it has been shown that thermal disassembly of the Ff virion and subsequent denaturation of its subunit α-helical structure are sufficient to generate a more canonical tyrosyl doublet in the Raman interval 820−860 cm^{-1} (*9*).

A similar situation applies to the filamentous virus Pf1. Each of the two tyrosines of the Pf1 coat subunit (Tyr 25 and Tyr 40) generates an apparent singlet at ∼854 cm^{-1} in the 820−860 cm^{-1} interval of the Raman spectrum (*25*). We conclude, therefore, that phenoxyl groups of both Tyr 25 and Tyr 40 in Pf1, like those of Tyr 21 and Tyr 24 in Ff, do not engage in significant hydrogen bonding in the assembled virion. Again, this may be a consequence of subunit packing in the assembled virus, which presumably traps the tyrosyl side chains in environments unfavorable to phenoxyl hydrogen-bonding interactions.

Relevance to Other Proteins. Although the Raman signature of the non-hydrogen-bonded phenoxyl ($I_2/I_1 = 6.7$) is distinct from that of the hydrogen-bonded phenoxyl ($0.3 < I_2/I_1 < 2.5$), the former would be difficult to identify in a protein containing both types of tyrosines. In fact, the tyrosyl signature with $I_2 \gg I_1$ has been demonstrated only for coat protein subunits of filamentous viruses Ff and Pf1, where all tyrosines are evidently of the non-hydrogen-bonded type. Nevertheless, we anticipate that a tyrosyl Raman singlet may be identified in future protein studies. Likely candidates are proteins consisting of α-helix bundles with tightly packed hydrophobic interfaces, wherein tyrosine phenoxyls may be restricted from forming hydrogen bonds with solvent molecules or other polar groups. This structural model, which apparently applies to the assembled coat subunits of Ff and Pf1 (*14*, *15*), may well apply to certain membrane-spanning helices. As noted above, the coat subunits of filamentous viruses indeed exhibit many properties typical of transmembrane α-helices (*13*).

The extant literature of protein Raman spectroscopy is weighted overwhelmingly toward the study of water-soluble globular proteins, as opposed to membrane proteins (*4*, *5*). In addition, the few membrane proteins examined previously contain tyrosines that are distributed among both transmembrane (solvent-protected) and peripheral (solvent-exposed) domains. For the reasons indicated above, the identification of a subset of non-hydrogen-bonded tyrosines in such proteins by Raman spectroscopy would be highly problematic. Accordingly, the apparent under-representation of non-hydrogen-bonded tyrosines among previously investigated proteins is not surprising.

CONCLUSIONS

A non-hydrogen-bonded phenoxyl group has been demonstrated for the tyrosyl model compound *p*-cresol in the vapor phase at 300 °C. Under these conditions, the phenoxyl Raman signature is distinguished by a Fermi doublet (839/812 cm^{-1}) with an extraordinarily high intensity ratio ($I_2/I_1 = 6.7$), which provides a basis for structural interpretation of previously reported Raman signatures of the filamentous viruses Ff and Pf1 (*8*, *25*). The results presented here also have broad implications for future use of Raman spectroscopy as a probe of tyrosyl hydrogen bonding in proteins (*2*).

The long-standing proposal of Siamwiza and co-workers (*2*), viz., that the Raman I_2/I_1 parameter serves as a reliable gauge of the average tyrosine hydrogen-bonding environment in a protein, was predicated upon the assumption that the phenoxyl group of each tyrosine is always hydrogen bonded, either as a donor, or as an acceptor, or as both a donor and an acceptor. Given this assumption, each phenoxyl is expected to generate a Fermi doublet with components (intensities) at approximately 830 ± 5 (I_1) and 850 ± 5 cm^{-1} (I_2) and with an intensity quotient I_2/I_1 between 0.30 and 2.5, depending upon the detailed hydrogen-bonding environment of each contributing phenoxyl. The present results indicate a need to modify and extend this proposition. Specifically, if the protein contains tyrosine phenoxyl groups that are not hydrogen-bonded, each such group can be expected to contribute to the composite Raman signature according to the ratio $I_2/I_1 = 6.7$. In a protein containing both hydrogen-bonded and non-hydrogen-bonded phenoxyls, the measured value of I_2/I_1 will comprise contributions from both types in accordance with their populations. Neglect of the non-hydrogen-bonded contributors will skew the measurement toward the upper limit of the hydrogen-bonded contributors and will not be representative of the average phenoxyl hydrogen-bonding environment in the protein.

Our results provide a structural basis for interpreting the apparent tyrosyl Raman singlets encountered for the Tyr 21 (851 cm^{-1}) and Tyr 24 (855 cm^{-1}) side chains in the coat protein subunit of the filamentous virus Ff. We propose that *the phenoxyl groups of Tyr 21 and Tyr 24 are not hydrogen-bonded in the virion assembly*. This conclusion is consistent with the hydrophobic environments inferred previously (*8*).

A similar situation applies to the subunit tyrosines, Tyr 25 and Tyr 40, in the class II filamentous virus Pf1. Each generates an apparent Raman singlet (∼854 cm^{-1}) rather than a canonical doublet (*25*). The locus of Tyr 25 in Pf1 is analogous to that of Tyr 21 and Tyr 24 in Ff, i.e., within the central hydrophobic region of the subunit. Although side chain packing in the vicinity of Tyr 40 is not known, the Raman singlet for this residue suggests an environment in which the *para* phenoxyl group also is *not* hydrogen-bonded in the usual sense. It is perhaps noteworthy that the position of Tyr 40 in the Pf1 subunit corresponds to that of Trp 38 in the subunit of the Pf3 virus and Trp 39 in the subunit of the Xf virus, both of which are architecturally similar (class II) to Pf1 (*26*). Interestingly, each of these aromatic side chains (Tyr 40 in Pf1, Trp 38 in Pf3, and Trp 39 in Xf) is characterized by anomalous Raman markers (*27*), and each may fulfill a similar unorthodox structural role. In the cases of Pf3 and Xf, the anomaly pertains to tryptophan and may be the result of cation−π interaction (*28*) involving the indolyl moiety and a neighboring basic side chain (*29*). Future studies will focus on determining whether a cation−π interaction may also be feasible for the aromatic ring of Tyr 40 in the Pf1 assembly.

REFERENCES

1. Lord, R. C., and Yu, N.-T. (1970) *J. Mol. Biol. 50*, 509−524.
2. Siamwiza, M. N., Lord, R. C., Chen, M. C., Takamatsu, T., Harada, I., Matsuura, H., and Shimanouchi, T. (1975) *Biochemistry 14*, 4870−4876.

3. Takeuchi, H., Watanabe, N., and Harada, I. (1988) *Spectrochim. Acta 44A*, 749−761.
4. Austin, J. C., Jordan, T., and Spiro, T. G. (1993) in *Biomolecular Spectroscopy, Part A* (Clark, R. J. H., and Hester, R. E., Eds.) Vol. 20, pp 55−127, John Wiley and Sons, New York.
5. Miura, T., and Thomas, G. J., Jr. (1995) in *Proteins: Structure, Function and Engineering* (Biswas, B. B., and Roy, S., Eds.) Subcellular Biochemistry, Vol. 24, pp 55−99, Plenum, New York.
6. Thomas, G. J., Jr. (1986) in *Spectroscopy of Biological Systems* (Clark, R. J. H., and Hester, R. E., Eds.) Advances in Spectroscopy, Vol. 13, pp 233−309, John Wiley and Sons, London.
7. Wen, Z. Q., and Thomas, G. J., Jr. (1998) *Biopolymers 45*, 247−256.
8. Overman, S. A., Aubrey, K. L., Vispo, N. S., Cesareni, G., and Thomas, G. J., Jr. (1994) *Biochemistry 33*, 1037−1042.
9. Overman, S. A., and Thomas, G. J., Jr. (1995) *Biochemistry 34*, 5440−5451.
10. Overman, S. A., and Thomas, G. J., Jr. (1998) *J. Raman Spectrosc. 29*, 23−29.
11. Wen, Z. Q., Overman, S. A., and Thomas, G. J., Jr. (1997) *Biochemistry 36*, 7810−7820.
12. Almeida, F. C. L., and Opella, S. J. (1997) *J. Mol. Biol. 270*, 481−495.
13. Marvin, D. A. (1998) *Curr. Opin. Struct. Biol. 8*, 150−158.
14. Symmons, M. F., Welsh, L. C., Nave, C., Marvin, D. A., and Perham, R. N. (1995) *J. Mol. Biol. 245*, 86−91.
15. Marvin, D. A., Hale, R. D., Nave, C., and Citterich, M. H. (1994) *J. Mol. Biol. 235*, 260−286.
16. McDonnell, P. A., Shon, K., Kim, Y., and Opella, S. J. (1993) *J. Mol. Biol. 233*, 447−463.
17. Finer-Moore, J., Stroud, R. M., Prescott, B., and Thomas, G. J., Jr. (1984) *J. Biomol. Struct. Dyn. 2*, 93−100.
18. Haller, K., Chiang, W. Y., del Rosario, A., and Laane, J. (1996) *J. Mol. Struct. 379*, 19−23.
19. Pimentel, G. C., and McClellan, A. L. (1960) *The Hydrogen Bond*, W. H. Freeman, San Francisco.
20. Sakurai, S. (1999) Ph. D. Thesis, Texas A&M University, College Station, TX.
21. Jakobsen, R. J. (1965) *Spectrochim. Acta 21*, 433−441.
22. Frisch, M. J., Trucks, G. W., Schlegel, H. B., Scuseria, G. E., Robb, M. A., Cheeseman, J. R., Zakrzewski, W. G., Montgomery, J. A., Jr., Stratmann, R. E., Burant, J. C., Dapprich, S., Millam, J. M., Daniels, A. D., Kudin, K. N., Strain, M. C., Farkas, O., Tomasi, J., Barone, V., Cossi, M., Cammi, R., Mennucci, B., Pomelli, C., Adamo, C., Clifford, S., Ochterski, J., Petersson, G. A., Ayala, P. Y., Cui, Q., Morokuma, K., Malick, D. K., Rabuck, A. D., Raghavachari, K., Foresman, J. B., Cioslowski, J., Ortiz, J. V., Stefanov, B. B., Liu, G., Liashenko, A., Piskorz, P., Komaromi, I., Gomperts, R., Martin, R. L., Fox, D. J., Keith, T., Al-Laham, M. A., Peng, C. Y., Nanayakkara, A., Gonzalez, C., Challacombe, M., Gill, P. M. W., Johnson, B., Chen, W., Wong, M. W., Andres, J. L., Gonzalez, C., Head-Gordon, M., Replogie, E. S., and Pople, J. A. (1998) *GAUSSIAN 98, Revision A.3*, Gaussian, Inc., Pittsburgh, PA.
23. Hameka, H. F., and Jensen, J. O. (1995) *THEOCHEM 331*, 203−214.
24. Lagant, P., Gallouj, H., and Vergoten, G. (1995) *J. Mol. Struct. 372*, 53−68.
25. Wen, Z. Q., Armstrong, A., and Thomas, G. J., Jr. (1999) *Biochemistry 38*, 3148−3156.
26. Day, L. A., Marzec, C. J., Reisberg, S. A., and Casadevall, A. (1988) *Annu. Rev. Biophys. Biomol. Struct. 17*, 509−539.
27. Thomas, G. J., Jr., Prescott, B., and Day, L. A. (1983) *J. Mol. Biol. 165*, 321−356.
28. Gallivan, J. P., and Dougherty, D. A. (1999) *Proc. Natl. Acad. Sci. U.S.A. 96*, 9459−9464.
29. Wen, Z. Q., and Thomas, G. J., Jr. (2000) *Biochemistry 39*, 146−152.

BI0023753